Navigation Using High-Frequency Ground Beacons and Ionosphere Model Corrections

Yoav Baumgarten and Mark L. Psiaki

Cornell University, Ithaca, NY 14853-7501, USA

BIOGRAPHIES

Yoav Baumgarten is a Ph.D. candidate in the School of Mechanical and Aerospace Engineering. He received a B.Sc. in Aerospace Engineering from the Technion – Israel Institute of Technology. His interests are in the areas of GNSS technology and applications, joint navigation and ionosphere characterization using HF beacons, and integrated navigation.

Mark L. Psiaki is a Professor of Mechanical and Aerospace Engineering. He received a B.A. in Physics and M.A. and Ph.D. degrees in Mechanical and Aerospace Engineering from Princeton University. His research interests are in the areas of GNSS technology and applications, alternatives to GNSS navigation, spacecraft attitude and orbit determination, and general estimation, filtering, and detection.

ABSTRACT

A new navigation concept is developed that relies on passive one-way ranging using pseudorange measurements of High-Frequency (HF) beacon signals that are reflected off of the ionosphere. This concept is being developed as a possible alternative to GNSS positioning and timing services, with clear benefits where it comes to costs and system redundancy. The proposed system's HF signals are transmitted from ground-based beacons. They travel from the known beacon locations to the unknown user equipment (UE) location along ray paths that reflect off of the Earth and the ionosphere. This reliance on reflected signals allows the beacons to lie beyond the receiver's horizon. If a set of beacon signals reaches the UE receiver with sufficient geometric diversity, then the three-dimensional position and the clock offset of the receiver can be determined. Ionospheric modeling uncertainty can cause large errors in the deduced UE position and clock offset. This can be compensated by developing a parametric model of ionosphere variability and by estimating corrections to these parameters as an integral part of the navigation solution. A batch filter is developed to estimate the UE position, clock offset, and corrections to an *a priori*

ionosphere model. This paper presents and initial evaluation of this concept. It analyzes the observability and possible accuracy of this system. For a case study involving significant errors in the *a priori* ionospheric parameters, the total error in position estimate was in an order of hundreds of meters in the horizontal plane and a couple of meters in the vertical direction. The *a posteriori* estimates for the ionosphere exhibits significantly smaller errors compared to the *a priori* data.

I. INTRODUCTION

The use of High Frequency (HF) signals propagating in the atmosphere has been widely discussed in the literature for communications and over-the-horizon radar. Signals with frequencies in the range 2-10 MHz can bounce successively off the ionosphere and the Earth to arrive at a receiver along a non-Line-Of-Sight (LOS) path. Such signals have been proposed for geolocation purposes, as in Ref. 1. The present paper represents a further effort to use such signals for radio navigation.

Given perfect knowledge of the ionosphere and of the number of bounces between a transmitter and a receiver, it is possible to develop a pseudorange model of the measured group delay that involves the unknown user receiver location and that receiver's unknown clock offset. Given 4 or more such pseudoranges from 4 or more independent transmitters with an appropriately diverse geometry, it should be possible to solve for the unknown user position and clock offset, similar to GPS.

The problem with such an approach is that the ionosphere's HF signal propagation/refraction/reflection properties are highly uncertain due to the variability of its 3-dimensional electron density distribution, $N_e(\underline{r})$. The approach of Ref. 1 is to use ionosonde data in order to refine a local model of $N_e(\underline{r})$. This local model is then used to estimate the unknown location of a transmitter. The present approach seeks to estimate simultaneously the location of an unknown receiver, its clock offset, and corrections to the relevant portions of the $N_e(\underline{r})$ distribution. Its input data are the measured group delays

between an array of transmitters at known locations and the user receiver.

The approach involves several elements. They are 1) a nominal ionosphere model, 2) estimated corrections to that model, 3) ray-tracing calculations for the paths of the HF signals from the transmitters to the receiver through the corrected model, and 4) model inversion calculations that update the user receiver position and clock offset estimates along with ionosphere correction estimates. These model inversion calculations are carried out using standard nonlinear least-squares techniques.

A key question for such an approach concerns observability. Given a limited number of transmitters and a limited number of measured group delays/pseudoranges, can such a system accurately estimate the many unknowns? The infinite-dimensional nature of ionospheric corrections, which exist in $N_e(\underline{r})$ function space, theoretically dooms such an approach to failure. In practice, however, it may be possible to combine *a priori* information about $N_e(\underline{r})$ with measured pseudoranges in order to arrive at a reasonable result. This paper represents an initial study of whether this might be practically possible.

One might try to conduct such a study using a complicated 3-dimensional electron density profile $N_e(\underline{r})$ and precise ray-tracing calculations, as in Ref. 2. For this early stage of feasibility analysis, one would like to avoid the significant complexity involved in incorporating the ray tracing model into both the algorithm and the simulation environment. One would prefer a simplified model that retains enough realism in the electron density profiles and in the refraction physics in order to yield a sensible indication of possible system performance. The current study utilizes just such a simplified model. A Chapman vertical profile with horizontal variations of its 3 parameters is used to model $N_e(\underline{r})$. The ray paths of the bouncing HF signals are presumed to be reflected off of this ionosphere model when conditions based on Snell's law are satisfied. The bounce height is a function of frequency, angle of incidence to a surface of constant $N_e(\underline{r})$, and the actual $N_e(\underline{r})$ value. Based on experience using this simplified refraction model as a first-guess generation method for ray-tracing solutions, the authors expect that a planned later study involving full ray-tracing calculations will exhibit performance somewhat similar to that achieved by the simplified model of the present study.

Thus, the basic question of the present study concerns whether, and to what extent, the joint estimation of position, receiver clock offset, and corrections to ionosphere parameters is possible. While it is well known that positioning is possible with a minimal number of received signals for the simpler satellite-based GPS problem, for the problem discussed here the increase in the number of unknowns and the convoluted manner those unknowns are related to the measured pseudoranges makes performance hard to predict based on simple analysis. Instead, performance must be studied using a complicated truth model simulation and a corresponding batch estimator.

This paper makes four contributions to the area of radio navigation based on bouncing HF signals. First, it develops a simplified measurement model of the group delays of multi-bounce HF signal paths from known beacon transmitter locations to an unknown user receiver location. This model includes techniques for solving its nonlinear bounce conditions and for computing first-partial derivative sensitivities of the bounces and the group delays with respect to the unknown user location and the unknown ionosphere parameters. Second, this paper develops a batch nonlinear least-squares estimation algorithm for determining the unknown user receiver position, user receiver clock offset, and ionospheric parameter corrections. This algorithm incorporates *a priori* information about the ionosphere parameters in order to compensate for the lack of strict simultaneous observability of the location, clock offset, and ionosphere corrections. Third, this paper develops a truth-model simulation to test its HF navigation scheme. Fourth, this paper evaluates the potential performance of its proposed HF navigation scheme using data from its truth-model simulation.

The remainder of this paper is divided into four sections plus conclusions. Section II presents the physical and mathematical models of the ionosphere and the bouncing HF signals. It covers the derivation and solution for the bounce points equation, the measurement model sensitivities, and the stacked measurements model. In Section III develops the batch filter that estimates the quantities of interest. It develops two different iterative solution strategies, one that applies when the current guess is far from the solution and another that applies near the solution. Section IV discusses the truth-model simulation used to evaluate this concept, and it presents performance analyses for three test cases. The findings of these analyses are further discussed in Section V, and plans for a follow-on study are outlined. Section VI summarizes this paper's developments, and it draws conclusions about the proposed new system.

II. PHYSICAL AND MATHEMATICAL MODELS

A. The Earth and the Ionosphere

Models of the Earth and the ionosphere are needed in order to trace HF bounce paths using the geometric optics calculations of perfect specular reflection. The Earth's surface is modeled as being the WGS-84 ellipsoid.

A three-parameter Chapman electron density model is assumed for the ionosphere. This model regards the ionosphere as a medium with an altitude-dependent

electron density whose altitude density distribution varies with latitude and longitude:

$$N_e(\underline{r}) = \frac{VTEC[\phi(\underline{r}),\lambda(\underline{r})]}{e \cdot h_{sf}[\phi(\underline{r}),\lambda(\underline{r})]} e^{\left(1-z(\underline{r})-e^{-z(\underline{r})}\right)}$$

$$z(\underline{r}) = \frac{h_{alt}(\underline{r}) - h_{max}[\phi(\underline{r}),\lambda(\underline{r})]}{h_{sf}[\phi(\underline{r}),\lambda(\underline{r})]}$$

(1)

where $\phi(\underline{r})$, $\lambda(\underline{r})$ and $h_{alt}(\underline{r})$ are, respectively, the latitude, longitude, and altitude above the WGS84 ellipsoid of the Cartesian ECEF position $\underline{r}$. $h_{max}[\phi(\underline{r}),\lambda(\underline{r})]$ is a parameter representing the altitude at which the maximal electron density is obtained. $VTEC[\phi(\underline{r}),\lambda(\underline{r})]$ is the vertical total electron content – the vertical integral of the electron density, and $h_{sf}[\phi(\underline{r}),\lambda(\underline{r})]$ is the profile's altitude scale height.

HF signals are assumed to reflect off of the ionosphere in a perfect specular manner. A reflection will occur when the angle ψ_0 of incidence with respect to the local unit normal vector $\underline{u} = -\nabla N_e(\underline{r})/\|\nabla N_e(\underline{r})\|$ and the local index of refraction n satisfy Snell's law such that the angle of the refracted signal ψ_1 equals 90^0, thus resulting in reflection rather than refraction. This condition incorporates an approximation for the vertical variations of n so that it is assumed to equal 1 below the reflection point and to transition abruptly to its value dictated by $N_e(\underline{r})$ at the reflection point. These assumptions lead to the following version of Snell's law for the reflection condition:

$$1 \cdot \sin(\psi_0) = n \cdot \sin(90^0)$$

(2)

At a reflection point the phase index of refraction depends on electron density $N_e(\underline{r})$ and on the signal's frequency ω. This dependency takes the form:

$$n(\underline{r}) = \sqrt{1 - C_1 \frac{N_e(\underline{r})}{\omega^2}} \quad , \quad C_1 = 3182.73849408628$$

(3)

Where $N_e(\underline{r})$ is given in units of electrons/m^3 and ω is given in units of radians/sec.

The latitude/longitude variations of the three Chapman vertical profile parameters are modeled using bi-quintic splines. The spline nodes are placed at predefined latitudes and longitudes with subsets of nodes grouped into common small circles of constant latitude. The defining parameters for each spline/mesh node are the given function's value and eight partial derivatives with respect to latitude ϕ and longitude λ. This a vector of 9 parameters $\underline{p}_i$ is associated with the ith node and splined function $a(\phi, \lambda)$ as follows:

$$\underline{p}_i = \left[a, \frac{\partial a}{\partial \lambda}, \frac{\partial a}{\partial \phi}, \frac{\partial^2 a}{\partial \lambda^2}, \frac{\partial^2 a}{\partial \lambda \partial \phi}, \frac{\partial^2 a}{\partial \phi^2}, \frac{\partial^3 a}{\partial \lambda^2 \partial \phi}, \right.$$
$$\left. \frac{\partial^3 a}{\partial \lambda \partial \phi^2}, \frac{\partial^4 a}{\partial \lambda^2 \partial \phi^2} \right]$$

(4)

Given the latitude ϕ_0 and the longitude λ_0 of a point at which one wants to compute the value of a Chapman parameter a (and possibly various of its partial derivatives), the needed calculations use the nearest four bi-quintic spline nodes that lie northwest, northeast, southwest, and southeast of (ϕ_0,λ_0). Stated differently, these 4 points lie on the two small circles of latitude which bracket ϕ_0. On each of these two small circles, the two chosen node points are those whose longitudes bracket λ_0.

The $a(\phi_0,\lambda_0;\underline{p})$ bi-quintic spline calculations proceed as follows: Suppose that (ϕ_i,λ_i) and (ϕ_j,λ_j) are the neighboring southwest and southeast biquintic spline nodes and that (ϕ_k,λ_k) and (ϕ_l,λ_l) are the neighboring northwest and northeast nodes. Then $\phi_i = \phi_j \le \phi_0 \le \phi_k = \phi_l$, $\lambda_i \le \lambda_0 \le \lambda_j$, and $\lambda_k \le \lambda_0 \le \lambda_l$. One uses the values of a_i, $(\partial a/\partial \lambda)_i$, and $(\partial^2 a/\partial \lambda^2)_i$ from the parameter vector $\underline{p}_i$ along with a_j, $(\partial a/\partial \lambda)_j$, and $(\partial^2 a/\partial \lambda^2)_j$ from the parameter vector $\underline{p}_j$ in a 1-dimensional quintic spline calculation in the longitude direction in order to determine $a(\phi_i,\lambda_0)$ on the lower small circle of latitude. The 9-element vectors $\underline{p}_i$ and $\underline{p}_j$ are the subsets of the whole-ionosphere parameter vector $\underline{p}$, subsets that apply at, respectively, nodes i and j. Similarly, two additional 1-dimensional longitude quintic spline calculations are used to determine $\partial a/\partial \phi$ at (ϕ_i,λ_0) based on $(\partial a/\partial \phi)_i$, $(\partial^2 a/\partial \phi \partial \lambda)_i$, $(\partial^3 a/\partial \phi \partial \lambda^2)_i$, $(\partial a/\partial \phi)_j$, $(\partial^2 a/\partial \phi \partial \lambda)_j$, and $(\partial^3 a/\partial \phi \partial \lambda^2)_j$ from $\underline{p}_i$ and $\underline{p}_j$ along with $\partial^2 a/\partial \phi^2$ at (ϕ_i,λ_0) based on $(\partial^2 a/\partial \phi^2)_i$, $(\partial^3 a/\partial \phi^2 \partial \lambda)_i$, $(\partial^4 a/\partial \phi^2 \partial \lambda^2)_i$, $(\partial^2 a/\partial \phi^2)_j$, $(\partial^3 a/\partial \phi^2 \partial \lambda)_j$, and $(\partial^4 a/\partial \phi^2 \partial \lambda^2)_j$ from $\underline{p}_i$ and $\underline{p}_j$. Corresponding 1-dimensional quintic spline calculations are repeated on the upper small circle of latitude in order to determine $a(\phi_k,\lambda_0)$, $\partial a/\partial \phi$ at (ϕ_k,λ_0), and $\partial^2 a/\partial \phi^2$ at (ϕ_k,λ_0). Finally, a 1-dimensional latitude quintic spline calculation is performed between the points (ϕ_i,λ_0) and (ϕ_k,λ_0) in order to determine the value of the Chapman model parameter at the original point: $a(\phi_0,\lambda_0)$. These calculations are facilitated by the fact that any 1-dimensional quintic spline is completely defined by the function, first-derivative, and second-derivative values at the spline interval's two end points.

B. Bounce Points, Ray-Paths, and the Measurement Model

A ray path is a sequence of ordered line segments. Each line segment is defined by its two end points. For a connected ray path of n line segments, $n+1$ points are defined as follows: The first point is the location of the transmitter, $\underline{q}$. The second point is a bounce point located on the ionosphere surface. All other bounce points are

alternately located on Earth and the ionosphere. The last point is the position of the receiver, $\underline{r}$. Bounce points are defined in their Earth Centered Earth Fixed (ECEF) representation, i.e. $[X_k;Y_k;Z_k]$.

Let ρ_j be the true length of the jth ray path that runs from the transmitter, alternately bounces off the ionosphere and the Earth, and eventually reaches the receiver. Let P_j be the measured pseudorange of that ray path, which equals the speed of light c multiplied the difference between the measured reception time according to the erroneous receiver clock and the true transmission time according to a calibrated beacon transmitter clock. Let δ be the receiver clock's offset. Then the jth measurement equation can be written as

$$P_j = h_j\left(\underline{x},\underline{p}\right) = \breve{h}_j\left(\underline{r},\underline{p}\right) + c\delta = \tilde{h}_j\left[\underline{r},\underline{\eta}_j\left(\underline{r},\underline{p}\right)\right] + c\delta \quad (5)$$

where the computed functions $\breve{h}_j$ and $\tilde{h}_j$ both model the true length of the jth ray-path, $\underline{\eta}_j$ is a vector containing the set of ECEF x-y-z coordinates of the ray-path's m-1 unknown bounce points:

$$\underline{\eta}_j = \left[X_1,X_2,...,X_{m-1},Y_1,Y_2,...,Y_{m-1},Z_1,Z_2,...,Z_{m-1}\right]^T \quad (6)$$

and the 4-dimensional unknown vector $\underline{x}$ = $[\underline{r};\ c\delta]$ contains the unknown receiver position and length-equivalent receiver clock offset.

The pseudorange model in Eq. (5) neglects the fact that refraction causes the signal to travel slower than the speed of light when near its reflection point in the ionosphere. This simplification would be unacceptable if dealing with real data. For purposes of the present study, however, the simplification is conjectured to be acceptable. It is conjectured not to degrade seriously this study's ability to test system observability and potential accuracy.

C. Bounce-Point Equations and Their Solution

Determination of the bouncing ray path that an HF signal traverses from a transmitter beacon to a receiver involves solution of coupled nonlinear equations which define the physical characteristics of its trajectory. Three equations are used to implicitly define each bounce point. For m segments there are m-1 unknown bounce points and therefore a set of 3(m-1) equations that serve to define these points. The set of 3 equations that defines the kth bounce point will be written in the form $0 = g_k(\underline{\eta}_j,\underline{p})$. Each of these equations is split into three scalar components, components of type A, B, and C, so that $g_k(\underline{\eta}_j,\underline{p})$ = $[g_{Ak}(\underline{\eta}_j,\underline{p});\ g_{Bk}(\underline{\eta}_j,\underline{p});\ g_{Ck}(\underline{\eta}_j,\underline{p})]$.

The kth Type-A constraint equation requires that the kth bounce point either lies on the Earth surface (even-valued k) or satisfies the ionospheric reflectivity condition (odd-valued k). For an even k, the corresponding equation is simply the implicit equation of the earth's surface in ECEF coordinates, $0 = g_{Ak}(\underline{\eta}_j,\underline{p}) = h_{WGS84}(X_k,Y_k,Z_k)$, where

$h_{WGS84}(X,Y,Z)$ is the function that calculates the altitude of Cartesian ECEF point (X,Y,Z) relative to the WGS-84 ellipsoid, as in Ref. 3. For an odd k, the Type-A equation considers the reflectivity condition that has been previously described. The form of the equation used here:

$$0 = g_{Ak}(\underline{\eta}_j,\underline{p})$$
$$= \left(\underline{v}_k{}^T\underline{u}\right)^2 - \frac{N_e\left(\underline{\eta}_j\right)}{\omega^2}\cdot C_1\left(\underline{v}_k{}^T\underline{v}_k\right)\left(\underline{u}^T\underline{u}\right) \quad (7)$$

where $\underline{v}_k$ is the incoming k^{th} ray-path line segment. The quantities $\underline{u}$, ω and, N_e are as defined earlier, with the vector $\underline{u}$ being directed along the normal to the local surface of constant N_e.

Type-B constraint equations enforce co-planarity for the incoming ray segment, the reflected ray segment and the normal vector to the Earth or ionosphere surface at the bounce point. For the kth bounce point, which links the kth ray path line segment and the $(k+1)^{st}$ ray-path line segment, the following equation definition for g_{Bk} applies:

$$0 = g_{Bk}(\underline{\eta}_j,\underline{p})$$
$$= \underline{u}_k\cdot(\underline{v}_k\times\underline{v}_{k+1}) \quad (8)$$

where for even numbered k $\underline{u}_k$ = $[\partial h_{altk}/\partial X_k;\ \partial h_{altk}/\partial Y_k;\ \partial h_{altk}/\partial Z_k]/[(\partial h_{altk}/\partial X_k)^2 + (\partial h_{altk}/\partial Y_k)^2 + (\partial h_{altk}/\partial Z_k)^2]^{0.5}$ is a unit vector perpendicular to the Earth's WGS-84 ellipsoid. This vector has previously been defined for ionosphere bounce points, i.e., for odd-numbered k. The vectors $\underline{v}_k$ and $\underline{v}_{k+1}$ are the incoming and reflected ray segments which are computed from $\underline{r}$, $\underline{p}$ and $\underline{\eta}_j$.

Type-C equations constrain the normal vector to the Earth or ionosphere surface at the bounce point to bisect to the angle between the incoming and reflected ray path line segments. It takes the form

$$0 = g_{Ck}(\underline{\eta}_j,\underline{p})$$
$$= \underline{u}_k\cdot(\|\underline{v}_{k+1}\|\underline{v}_k + \|\underline{v}_k\|\underline{v}_{k+1}) \quad (9)$$

The $g_k(\underline{\eta}_j,\underline{p})$ constraint functions for the m-1 bounce points can be stacked into a single column vector function of dimension 3m-3: $g(\underline{\eta}_j,\underline{p})$ = $[g_1(\underline{\eta}_j,\underline{p});g_2(\underline{\eta}_j,\underline{p});$ $g_3(\underline{\eta}_j,\underline{p});...;g_{m-1}(\underline{\eta}_j,\underline{p})]$. This leads to the following coupled system of 3m-3 nonlinear equations in the unknown 3m-3 elements of $\underline{\eta}_j$: $0 = g(\underline{\eta}_j,\underline{p})$. The final ray-path direction vector $\underline{v}_m$ depends on the unknown receiver position $\underline{r}$. It is important to recognize this $\underline{r}$ dependence. Thus, the final form of these coupled reflection conditions is $0 = g(\underline{\eta}_j,\underline{r},\underline{p})$.

The final constraint equation can be interpreted as defining the vector of unknown intermediate bounce points, $\underline{\eta}_j$, as an implicit function of the receiver position $\underline{r}$ and the ionospheric parameter vector $\underline{p}$. The

corresponding explicit function can be written formally as $\underline{\eta}_j(\underline{r},\underline{p})$.

The explicit function $\underline{\eta}_j(\underline{r},\underline{p})$ is evaluated numerically within this project's measurement model calculations. These calculations involve Newton's method. Given input values of $\underline{r}$ and $\underline{p}$, a first guess of the bounce points in $\underline{\eta}_j$ is constructed using the simple geometry of a spherical Earth and a constant-altitude ionosphere. Newton's method is then used to solve the nonlinear equation $0 = \underline{g}(\underline{\eta}_j,\underline{r},\underline{p})$ iteratively. Newton's method linearizes this equation about a given guessed value of $\underline{\eta}_j$, solves this linearized equation for an improved $\underline{\eta}_j$ guess, performs a line search between the old $\underline{\eta}_j$ guess and the new guess in order to guarantee a decrease in the sum of the squares of the equation errors, and repeats this entire procedure until the solution converges.

It has been demonstrated that for some combinations of $\underline{q}$ (the transmitter location), m, $\underline{r}$, and $\underline{p}$ a feasible solution for the intermediate bounce points vector $\underline{\eta}$ does not exist. For other combinations of $\underline{q}$, m, $\underline{r}$, and $\underline{p}$ it is possible that multiple solutions exist. In the latter case, an auxiliary algorithm is needed in order to determine which of the possible solutions corresponds to the actual measured pseudorange.

D. Calculation of Jacobian Matrices

Various first partial derivative Jacobian matrices of the $\underline{g}$ and $\tilde{h}_j$ functions are needed for this method's calculations. For example, the partial derivatives of $\underline{g}$ with respect to the elements of $\underline{\eta}$ are needed to implement the Newton's method solution of the equation $0 = \underline{g}(\underline{\eta},\underline{r},\underline{p})$ in order to compute the function $\underline{\eta}(\underline{r},\underline{p})$.

The calculation of many of these partial derivatives is straightforward. Special care should be taken, however, with the Jacobian $\partial \underline{g}/\partial \underline{\eta}$. Since some rows of $\underline{g}$ contain terms defined in Cartesian ECEF coordinates, geographic LLA coordinates and the partial derivatives of the geographic LLA coordinates with respect to the Cartesian ECEF coordinates, it is necessary to deal carefully with some entries of the Jacobian matrix. Additional complexity arises from the manner in which the $\underline{g}$ functions depend on the unknown $\underline{p}$ parameters which are used to compute the three Chapman profile parameters. Odd numbered $\underline{g}$ equations have been derived using the normal vector applying at an ionosphere reflection point which is defined as the negative gradient of the electron density field with respect to Cartesian ECEF coordinates. Computation of many of the needed partial derivatives involves partial differentiation with respect to the geographic latitude and longitude coordinates followed by partial differentiation of these coordinates with respect to Cartesian ECEF coordinates and application of the chain rule. The details for these partial derivative calculations have been omitted for the sake of brevity.

E. Measurement Model Sensitivity Matrices

Nonlinear gradient-based estimation algorithms, such as traditional batch least-squares, require partial derivatives of the measurement model with respect to the unknown estimated quantities. These sensitivities must be computed at a succession of improved guesses of the optimal estimates of the unknowns. In the present context, the required partial derivatives are those of each h_j measurement model function with respect to the elements of the unknown $\underline{x}$ and $\underline{p}$ vectors. The partial derivative with respect to the fourth element of $\underline{x}$, the $c\delta$ element, is 1, consistent with Eq. (5). The other derivatives, those with respect to the elements of $\underline{r}$ and $\underline{p}$ require special care.

Recalling the $\underline{g}$ system of equations $0 = \underline{g}\left[\underline{\eta}_j\left(\underline{r},\underline{p}\right),\underline{r},\underline{p}\right]$ and taking the partial derivative with respect to $\underline{r}$ while accounting for the dependence of $\underline{\eta}$ on $\underline{r}$ yields

$$\frac{\partial \underline{g}}{\partial \underline{\eta}_j}\frac{\partial \underline{\eta}_j}{\partial \underline{r}} + \frac{\partial \underline{g}}{\partial \underline{r}} = 0 \tag{10}$$

or

$$\frac{\partial \underline{\eta}_j}{\partial \underline{r}} = -\left[\frac{\partial \underline{g}}{\partial \underline{\eta}_j}\right]^{-1}\frac{\partial \underline{g}}{\partial \underline{r}} \tag{11}$$

Then the matrix of sensitivities of the jth measurement model group delay to errors in the estimate of the receiver's position is:

$$\begin{aligned}\frac{\partial \underline{h}_j}{\partial \underline{r}} = \frac{D\tilde{\underline{h}}_j}{D\underline{r}} &= \frac{\partial \tilde{\underline{h}}_j}{\partial \underline{\eta}_j}\frac{\partial \underline{\eta}_j}{\partial \underline{r}} + \frac{\partial \tilde{\underline{h}}_j}{\partial \underline{r}}\\ &= -\frac{\partial \tilde{\underline{h}}_j}{\partial \underline{\eta}_j}\left[\frac{\partial \underline{g}}{\partial \underline{\eta}_j}\right]^{-1}\frac{\partial \underline{g}}{\partial \underline{r}} + \frac{\partial \tilde{\underline{h}}_j}{\partial \underline{r}}\end{aligned} \tag{12}$$

Similarly, taking the partial derivative of the $\underline{g}$ equation with respect to $\underline{p}$ while accounting the dependence of $\underline{\eta}$ on $\underline{p}$ yields:

$$\frac{\partial \underline{g}}{\partial \underline{\eta}_j}\frac{\partial \underline{\eta}_j}{\partial \underline{p}} + \frac{\partial \underline{g}}{\partial \underline{p}} = 0$$

$$\Downarrow \tag{13}$$

$$\frac{\partial \underline{\eta}_j}{\partial \underline{p}} = -\left[\frac{\partial \underline{g}}{\partial \underline{\eta}_j}\right]^{-1}\frac{\partial \underline{g}}{\partial \underline{p}}$$

and the matrix of sensitivities of the jth modeled group delay to errors in the estimate of the ionospheric parameters is

$$\frac{\partial \underline{h}_j}{\partial \underline{p}} = \frac{D\tilde{\underline{h}}_j}{D\underline{p}} = \frac{\partial \tilde{\underline{h}}_j}{\partial \underline{\eta}_j}\frac{\partial \underline{\eta}_j}{\partial \underline{p}} + \underbrace{\frac{\partial \tilde{\underline{h}}_j}{\partial \underline{p}}}_{0}$$

$$= -\frac{\partial \tilde{\underline{h}}_j}{\partial \underline{\eta}_j}\left[\frac{\partial \underline{g}}{\partial \underline{\eta}_j}\right]^{-1}\frac{\partial \underline{g}}{\partial \underline{p}} \tag{14}$$

F. Stacked Measurement Model

The measurement model for each individual pseudorange takes the form given for the jth pseudorange in Eq. (5). For convenience in batch estimation, this model is stacked into an N-dimensional vector function model of all N measurements. It takes the form

$$\underline{h}(\underline{x},\underline{p}) = \begin{bmatrix} h_1(\underline{x},\underline{p}) \\ h_2(\underline{x},\underline{p}) \\ h_3(\underline{x},\underline{p}) \\ \vdots \\ h_j(\underline{x},\underline{p}) \\ \vdots \\ h_N(\underline{x},\underline{p}) \end{bmatrix} \tag{15}$$

It is straightforward to compute the Jacobian matrix of first partial derivatives of this vector function with respect to the $\underline{x}$ and $\underline{p}$ vectors. They are simply stacked collections of the individual row vectors $\partial h_j/\partial \underline{x}$ or $\partial h_j/\partial \underline{p}$ for $j = 1, \dots, N$.

III. BATCH ESTIMATION OF THE POSITION, RECEIVER CLOCK OFFSET AND IONOSPHERE PARAMETERS

A. Nominal Batch Filter Problem and Solution

A batch filter has been developed. It estimates $\underline{x}$ and $\underline{p}$ by minimizing a cost function that includes weighted squared differences between the measurements and their modeled values and between the estimated $\underline{p}$ elements and their *a priori* values. The batch filtering problem seeks the values that jointly minimize the cost function

$$J_1(\underline{x},\underline{p}) = \tfrac{1}{2}[\underline{P} - \underline{h}(\underline{x},\underline{p})]^{\mathrm{T}} R^{-1}[\underline{P} - \underline{h}(\underline{x},\underline{p})]$$
$$+ \tfrac{1}{2}(\underline{p} - \overline{\underline{p}})^{\mathrm{T}} M^{-1}(\underline{p} - \overline{\underline{p}}) \tag{16}$$

where $\underline{P}$ is the stacked vector of the N measured pseudoranges for the N ray paths, R is the square, symmetric, N-by-N, positive definite measurement error covariance matrix (typically a diagonal matrix), $\overline{\underline{p}}$ is the *a priori* estimate of the ionosphere parameter vector, and M is the square, symmetric, positive definite covariance matrix that models the uncertainty in the *a priori* ionosphere parameter vector $\overline{\underline{p}}$. The M matrix has row and column dimensions equal to the dimension of $\underline{p}$.

The batch least-squares cost function in Eq. (16) omits *a priori* values of the elements of $\underline{x} = [\underline{r};c\delta]$ and penalties for differences from those values for the estimated $\underline{x}$. This means that no prior knowledge about these terms is assumed, just as in standard GPS point navigation solutions.

The minimizing solution to the estimation problem in Eq. (16) is equivalent to the optimal least-squares solution to the following over-determined system of nonlinear equations:

$$\begin{bmatrix} R^{-1/2}\underline{P} \\ M^{-1/2}\overline{\underline{p}} \end{bmatrix} = \begin{bmatrix} R^{-1/2}\underline{h}(\underline{x},\underline{p}) \\ M^{-1/2}\underline{p} \end{bmatrix} + \underline{v}_1 \tag{17}$$

where $R^{-1/2}$ and $M^{-1/2}$ are the inverses of the Cholesky factor square roots of, respectively, the matrices R and M and where $\underline{v}_1$ is a zero-mean, identity-covariance Gaussian random error vector whose norm squared is minimized by the solution.

The Gauss-Newton method has been used to solve this estimation problem. This method is described in Ref. 4. It is a gradient-based iterative method. Each iteration starts with guesses of the optimizing values of $\underline{x}$ and $\underline{p}$. First it linearizes Eq. (17) about these guessed values. Next it solves the resulting over-determined linear least-squares problem to get candidates for improved solution guesses of $\underline{x}$ and $\underline{p}$. Finally, it searches along the line in $[\underline{x};\underline{p}]$ space from the old guess to the candidate new guess in order to find a new guess that reduces the cost $J_1(\underline{x},\underline{p})$. This process repeats until the cost is minimized. The line search between the old guess and the new candidate guess, if implemented well, ensures convergence to a local minimum of $J_1(\underline{x},\underline{p})$.

Recognizing the limitations of the first-order Gauss Newton method when it comes to arriving at a solution starting from a guess that is far from the receiver's true location, the algorithm distinguishes between two cases. In Case 1, the position solution is assumed to be close to convergence. In this case the algorithm will consider variations in the three components of the ECEF representation of the receiver's location $\underline{r}$, variations in the range-equivalent receiver clock offset $c\delta$, and variations in the ionosphere parameters of all bi-quintic spline nodes that affect the bounce points. In Case 2 the position solution is assumed to be far from convergence. A special algorithm has been developed for this case.

B. Iterating When Position Solution is Far From Convergence

In Case 2 the algorithm only considers variations in the receiver position's latitude and longitude and variations of clock bias. Variations of altitude and of ionospheric model parameters are excluded. The authors' experience has demonstrated that this ad hoc fix, when starting far from the solution, tends to ensure convergence. The

simplified cost function for this simplified search takes the following form:

$$J_2(\underline{x}) = \tfrac{1}{2}[\underline{P} - \underline{h}(\underline{x}, \underline{p})]^T R^{-1}[\underline{P} - \underline{h}(\underline{x}, \underline{p})] \qquad (18)$$

The corresponding over-determined system of equations in linearized latitude/longitude form is

$$R^{-1/2}[\underline{P} - \underline{h}(\underline{x}_g, \underline{p})] =$$

$$R^{-1/2} \left. \frac{\partial \underline{h}}{\partial \underline{x}} \right|_{(\underline{x}_g, \underline{p})} \begin{bmatrix} \frac{\partial r}{\partial \phi} & \frac{\partial r}{\partial \lambda} & 0 \\ 0 & 0 & 1 \end{bmatrix} \begin{bmatrix} \Delta\phi \\ \Delta\lambda \\ \Delta(c\delta) \end{bmatrix} + \underline{v}_2 \qquad (19)$$

where $\underline{x}_g = [r(\phi_g, \lambda_g, h_{altg}); (c\delta)_g]$ is the guessed solution vector for the receiver position and clock offset, with the position being dictated by the guessed WGS-84 latitude ϕ_g, longitude λ_g, and altitude h_{altg}. The latter quantity remains fixed during this initial part of the optimization, but ϕ_g and λ_g get updated as does $(c\delta)_g$. Their updates are the increments that are solved for in the over-determined linearized system of equations in Eq. (19). Re-scaled increments are used, if necessary, in order to ensure that $J_2(x)$ from Eq. (18) decreases for each increment.

C. Theoretical Estimation Error Covariance

The use of inverse covariance matrixes in the cost function in Eq. (16) implies that its second derivative Hessian matrix at the truth solution can be inverted in order to compute the Cramer-Rao lower bound for the estimation error covariance. This matrix characterizes the potential accuracy of a very good estimator. It is useful for determining whether the proposed system has any potential to produce accurate navigation solutions. If the square roots of the diagonal elements of this covariance lower-bound are too large, then this system will not work well. If they are small, then the system has the potential to work well. This covariance lower bound takes the form:

$$E\left(\begin{bmatrix} \Delta\underline{x} \\ \Delta\underline{p} \end{bmatrix} \cdot \begin{bmatrix} \Delta\underline{x} \\ \Delta\underline{p} \end{bmatrix}^T \right)$$

$$= \left(\begin{bmatrix} \frac{\partial \underline{h}}{\partial \underline{x}} & \frac{\partial \underline{h}}{\partial \underline{p}} \end{bmatrix}^T \begin{bmatrix} R & 0 \\ 0 & M \end{bmatrix}^{-1} \begin{bmatrix} \frac{\partial \underline{h}}{\partial \underline{x}} & \frac{\partial \underline{h}}{\partial \underline{p}} \end{bmatrix} \right)^{-1} \qquad (20)$$

The 3x3 top left block of this matrix represents the covariance associated with the position estimate in ECEF coordinates. With the appropriate transformation it can be converted into errors in the north-east-vertical coordinates. The 4x4 top left block represents the covariance associated with $\underline{x} = [\underline{r}; c\delta]$. An appropriately normalized square root of its trace constitutes this system's geometric dilution of precision (GDOP).

IV. SIMULATION AND PERFORMANCE

A. Truth-Model Simulation

A MATLAB truth-model simulation has been developed for algorithm assessment and performance analysis. It enables testing any desired combination of ground stations array, ray-path characteristics, measurement error models, and other parameters. It should be noted, however, that not all such combinations are physically feasible. For some cases, trying to solve for the $\underline{\eta}$ terms given $\underline{p}$ and $\underline{r}$ would result in no valid solution. Feasibility of the given configuration is tested during the first stage of the simulation execution.

Computation for an $N_e(\underline{r})$ truth model utilizes a Chapman profile that is fit to the International Reference Ionosphere (IRI) model for a particular time and date. This manner of generating a truth electron density model is thought to be reasonably representative of a possible real spatial electron density distribution.

The simulation uses "truth" values of the $\underline{x}$ and $\underline{p}$ vectors in the vector pseudorange measurement model of Eq. (15). It adds to these measurements a random error vector that is sampled from a zero-mean Gaussian distribution with covariance matrix R, consistent with the batch least-squares problem definition.

The simulation also generates an *a priori* estimate of the ionosphere parameter vector for use in the cost function of Eq. (16). This *a priori* $\bar{p}$ vector differs from the "truth" $\underline{p}$ vector in significant ways. The method of generating appropriate differences, perhaps differences that are even a bit larger than one would be expect in a real situation, is to use the IRI model with a 3-6 months date difference to generate $\bar{p}$ via Chapman-profile fitting versus the date used to generate the "truth" $\underline{p}$ using the same fitting technique. Such a choice ensures that the truth-model simulation is not using an unreasonably optimistic model of how well the filter's known $\bar{p}$ would approximate the truth ionosphere. The corresponding M parameter uncertainty covariance matrix has been sized to be consistent with the difference between the filter's *a priori* $\bar{p}$ and the "truth" $\underline{p}$ that has been used to generate the simulated measurements.

B. Test Case A Results

Test Case A considers an array of eleven ground stations spread at various locations across the US. A receiver, located at latitude/longitude/altitude (LLA) $[40^0, -95^0, 10000_m]$, i.e., at the center of the green spider-like object in Fig. 1. It receives three signals from each ground station to yield a total of thirty three signals received. The true ionosphere surface is based on IRI data computed for Jan. 23, 2010 at UTC 2:22 p.m. The *a priori* model is based on data computed for Oct. 23, 2009

at the same hour. The HF signals for this case have frequencies in the range 4.6-5.4 MHz.
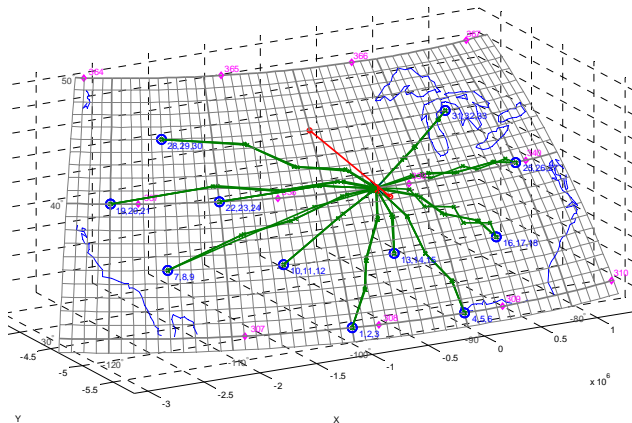
Figure 1: Setup and convergence of position solution for Case A.

Figure 1 illustrates the setup for Test Case A. The blue circles denote ground stations (with the corresponding broadcast signals' identifying j indices). The segmented green lines are the true ray-paths computed by the simulation. The magenta diamonds denote ionosphere bi-quintic spline nodes (with their identifying numbers). The North American coastline is shown as a thin blue line.

The red line shown on Fig. 1 illustrates the Gauss Newton algorithm's convergence performance. It plots a history of successive receiver position solution guesses. It is evident that the position estimate converges from an initial guess with a significant error to the receiver's true position. A closer look at the estimated values indicates that the final position error in this case is 203 meters in the local north direction, 600 meters in the local east direction, and 5 meters in the vertical direction. The error in the estimate of the receiver clock bias is equivalent to 1015 meters. At the same time, the computed Cramer-Rao covariance matrix lower bound contains 1-σ errors of 5468 meters north, 4776 meters east, and 177 meters vertical. One would expect larger actual estimation errors with such large computed σ values. The relative smallness of the actual errors may indicate that the chosen *a priori* error covariance for the ionospheric parameter vector, the matrix *M*, is too large.

Figure 2 plots errors between the *a priori* (top) and *a posteriori* (bottom) estimates of the ionospheric peak electron density altitude h_{max} parameter and the true ionosphere h_{max} parameter. The red square indicates the true position of the receiver. Blue circles with white edges denote the locations of the ground stations. Magenta diamonds denote the locations of the predefined grid nodes. The green dots mark computed ionospheric bounce points. North America's coastline is shown in white with the borders of the states shown in gray.

It is evident that the initial errors in h_{max} have been reduced dramatically, from up to 18 km to less than five

kilometer above the majority of the continental US. At the same time, significant errors of up to 7 km for the ionospheric scale height parameter h_{sf} have been reduced at the expense of some degradation near the true position of the receiver, as demonstrated in Fig. 3.
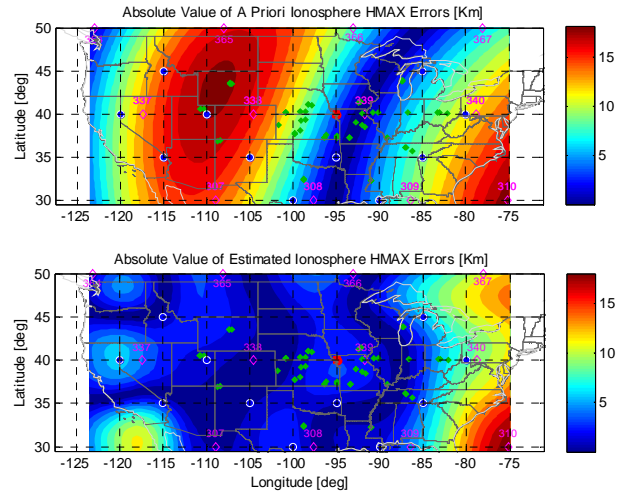
Figure 2: *A priori* (top) and *a posteriori* (bottom) errors for the ionospheric h_{max} parameter for Case A.
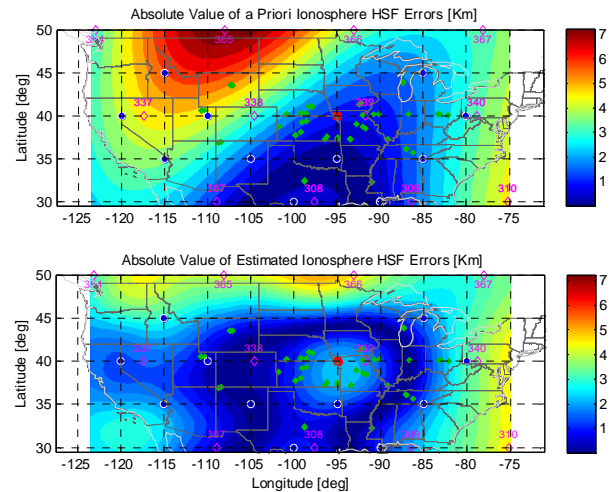
Figure 3: *A priori* (top) and *a posteriori* (bottom) errors for the ionospheric h_{sf} parameter for Case A.

Finally, a significant reduction in errors for the *VTEC* parameter have been achieved, as shown on Fig. 4. Note, however, that for the given ray-path length measurements, *VTEC* errors are observable only at heights that are less than the height for which maximal electron density is obtained, i.e. h_{max}. In other words, the observable part of *VTEC* is only that part of the *VTEC* integral up to the altitude of peak electron density.

C. Test Case B Results

In Test Case B greater initial errors for the *a priori* ionosphere model have been used. The *a priori* vector *p* has been computed using IRI data applying on Sept. 23,

8

2009, while the truth-model ionosphere *p* vector still comes from Jan. 23, 2010. Thus, the seasonal discrepancy has been increased from 3 months to 4 mouths. This case also uses a wider range of frequencies, 4.2-7.8 MHz.
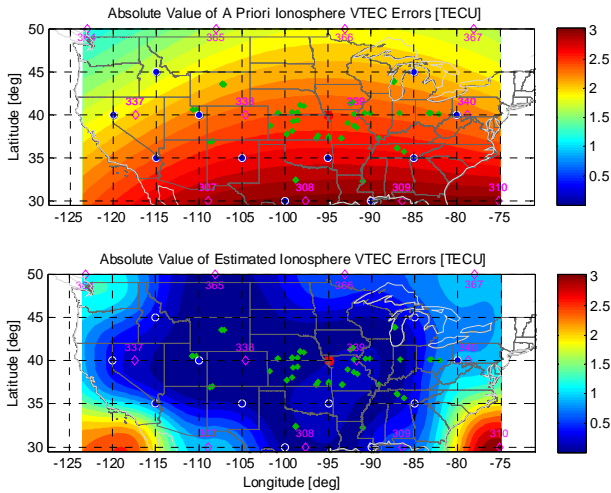
Figure 4: *A priori* (**top**) and *a posteriori* (**bottom**) errors for the ionospheric *VTEC* parameter for Case A.

Final positioning errors for this case were 519 meters north, 511 meters east, and 20 meters in the vertical direction. This case's performance for estimating two of the three Chapman profile parameters is shown in Figs. 5 and 6. A comparison of Figs. 2 and 5 shows that the *a priori* h_{max} errors are larger for this case relative to Case A (top plots of the two figures), while the final estimates for Cases A and B have roughly comparable accuracies (bottom plots of the two figures). A comparison of Figs. 3 and 6 yields similar conclusions for the *a priori* and final estimates of the h_{sf} errors for Cases A and B.
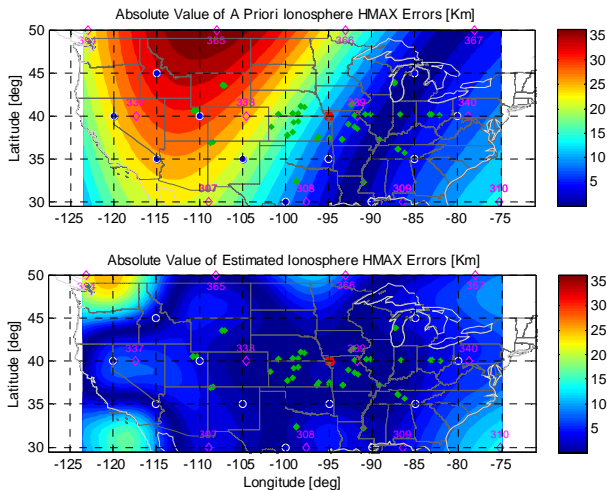
Figure 5: *A priori* (**top**) and *a posteriori* (**bottom**) errors for the ionospheric h_{max} parameter for Case B.
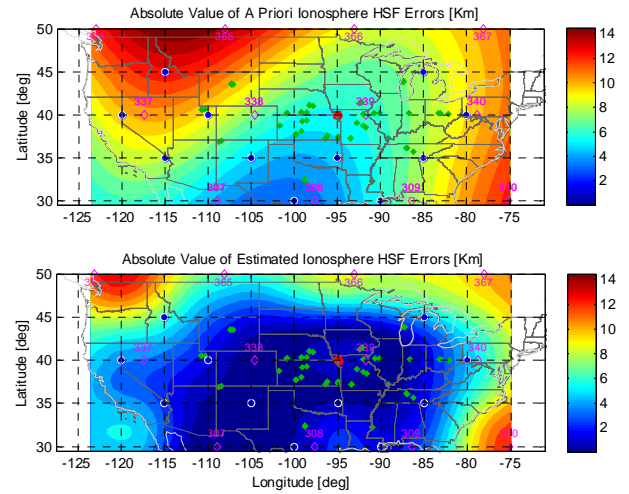
Figure 6: *A priori* (**top**) and *a posteriori* (**bottom**) errors for the ionospheric h_{sf} parameter for Case B.

D. Test Case C Results

In Test Case C fewer ground stations and fewer received signals have been considered. All other parameters including signals' frequencies are unchanged from Test Case A. Fig. 7 illustrates the setup for this case.
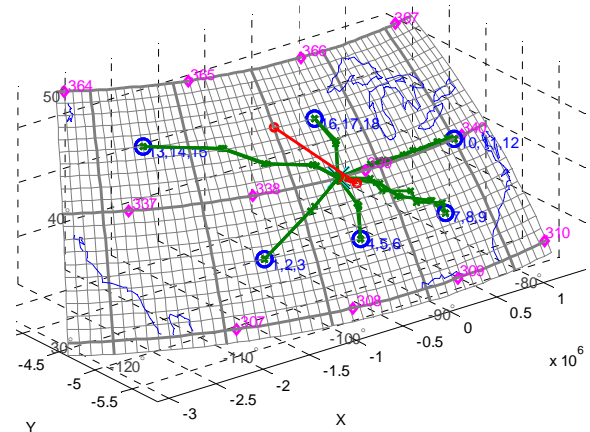
Figure 7: Setup and convergence of position solution for Case C.

Positioning errors for this test case were 1327 meters north, 1526 meters east, and 171 meters vertical. The error in the estimate for the receiver clock offset is equivalent to 5828 meters. The computed Cramer-Rao standard deviations for the positioning error components are 9823 meters north, 11238 meters east, and 442 meters vertical. Again, the computed σ values are significantly greater than the actual errors, indicating a possible conservatism with the covariance matrix *M* of errors in the *a priori* ionosphere parameter estimate *p*. Note, however, that the simulated actual errors and the corresponding Cramer-Rao σ values are larger for this case in comparison to Case A. This makes sense based on the use of fewer ground stations and fewer received signals. Conversely, one would expect to achieve better

performance than in Case A if one were to increase the number of ground stations and the number of signals.

V. DISCUSSION AND FUTURE DIRECTIONS

The results for the three test cases presented in this paper suggest that the problem is sufficiently observable to make this a candidate for navigation. That is, a position solution can be obtained to a reasonable level of accuracy despite uncertainty about the ionosphere. At the same time, the filtered estimates of the ionosphere electron density profile parameters have significantly reduced errors in comparison to the *a priori* estimates. Unsurprisingly, improved results have been observed when more measurements are available, and a better match has been achieved along ray paths in this situation. The impact of having a wide range of signal frequencies is also evident.

In all cases, actual positioning errors are smaller than the corresponding σ values from the Cramer-Rao lower bound for the estimation error covariance matrix. This discrepancy is probably due to some of the terms of M being too big in an attempt to allow significant corrections to the parameters of the ionosphere model. An additional effort should be put into considering cross-correlation between the various terms of M. For example, the altitude perturbations of peak electron density at neighboring nodes are likely to be correlated.

Further investigations have shown that in all cases the solutions for the minimization problem indeed converge to their global minimum. Thus, the presence of nonlinearities in the problem model does not pose a significant challenge to solving the underlying batch estimation problem.

The cost function considers both measurement errors and normalized corrections to the ionospheric parameters. The latter cost terms are included in order to preclude the filter from making unreasonably large modifications to its *a priori* ionosphere model for the sake of achieving a better fit to the measured pseudoranges. Consequently small corrections to the ionospheric electron density distribution are favored over big corrections, potentially resulting in less accurate results for the position solution. The batch filter could be tuned to allow very large corrections to the ionosphere parameters by making its M matrix very large. Such a tuning would result in a very low optimal cost and in a good fit to the measured pseudoranges.   The authors' experience with similar estimation problems, however, indicates that the resulting position/clock estimates in the $\underline{x}$ vector could become highly inaccurate.

These results answer this study's initial feasibility question in the affirmative: The proposed technique can be used to navigate while simultaneously estimating corrections to the ionosphere. This answer suggests that

this should project proceed to its next planned study. That study is slated to use a more realistic ionosphere model and a precise ray-tracing engine for modeling the refractive propagation of the RF signals through the ionospheric medium. During this planned study, truth-model simulation tests could be supplemented with tests involving actual data from a network of HF beacons and receivers.   Such a network is being deployed in South America.

The propagation model of the next study will have advantages and disadvantages relative to the simplified model of the present study. A greater physical fidelity will be achievable using the enhanced ionospheric model and ray-tracing calculations. On the disadvantage side, the enhanced 3-dimensional nature of the $N_e(\underline{r})$ distribution will increase the number of estimated ionosphere parameters that will be needed in order to characterize differences between the *a priori* model and the true ionosphere. This increased number of parameters will complicate the filter task of simultaneously estimating receiver position, receiver clock offset, and ionosphere corrections. The authors conjecture that the advantages and disadvantages of the proposed new models will balance out and that similar or possibly better performance will be found in the planned more-realistic follow-on study.

The project may consider augmenting the estimation problem with additional types of fused data.   For example, data from ionosondes or GPS slant TEC data from a network of receivers might help to improve the estimates of the ionosphere model corrections. Any such improvements should also improve the receiver position and clock offset estimates. Of course, such a system would need a method of communicating the independent ionosphere data to the user receiver, which would complicate its infrastructure.

VI. SUMMARY AND CONCLUSION

A batch filter algorithm has been developed that utilizes pseudorange measurements from HF signals propagating in the ionosphere to solve a combined positioning/ ionosphere-corrections problem. These HF signals are transmitted from stationary ground-based beacons at known locations. They propagate to an over-the-horizon user receiver at an unknown location via multiple bounces off of the ionosphere and the Earth. The navigation filter estimates user position, user clock error, and corrections to parameters that characterize the ionosphere's 3-dimensional electron density profile. The performance of this system has been investigated using a truth-model simulation. The simulation and the corresponding filter use a simplified model of the refractive bounces of the HF signals off of the ionosphere.

Three simulated test cases have been considered. With a relatively dense array of transmitters and a corresponding

large number of received signals, positioning errors are on the order of hundreds of meters. Vertical position accuracy is the best. With about half the original number of signals, the total position error grows to about 2000 meters. In 3 all cases, errors in the *a priori* model for the ionosphere are reduced dramatically by the filter. These results indicate that the problem is observable and that navigation accuracy might be reasonably accurate given sufficient availability of received HF signals.

REFERENCES

[1] Huang, X., and Reinisch, B.W., "Real-Time HF Ray Tracing through a Tilted Ionosphere," *Radio Science*, Vol. 41, 2006, RS5S47, doi:10.1029/2005RS003378.

[2] Jones, R.M., and Stephenson, J.J., "A Versatile Three-Dimensional Ray Tracing Computer Program for Radio Waves in the Ionosphere," U.S. Dept. of Commerce, OT Report 75-76, Oct. 1975.

[3] Hofmann-Wellenhof, B., Lichtenegger, H., and Collins, J., "Global Positioning System: Theory and Practice", Springer Wien New York, (Austria 2001), pp. 279-282.

[4] Gill, P.E., Murray, W., and Wright, M.H., "Practical Optimization", Academic Press, (New York, 1981), pp. 133-139.